Effect of Jet Velocity on Metal Removal Ability of a Biomachining Solution and Its Mechanism

Weimin Lin[a, b], Hui Huang[a, b, c*], Weibin Shi[b], Fei Ma[d], Tukun Li[e], Iain Macleod[f]

[a]*Institute of Manufacturing Engineering, Huaqiao University, Xiamen 361021, China*

[b]*College of Mechanical Engineering and Automation, Huaqiao University, Xiamen 361021, China*

[c]*State Key Laboratory of High-performance Tools, Huaqiao University, Xiamen 361021, China*

[d]*School of Mechanical Engineering, Hubei Institute of Engineering, Xiaogan 430074, China*

[e]*EPSRC Future Advanced Metrology Hub, Centre for Precision Technologies, School of Computing and Engineering, University of Huddersfield, Huddersfield, HD1 3DH, UK*

[f]*IMA Ltd, 29 Clay Lane, Cheshire, WA15 8PJ, United Kingdom*

*. Corresponding author, E-mail: huangh@hqu.edu.cn, TEL: (+86) 18959260602, FAX: (+86) 05926162588

Abstract

Three metal (Fe, Co, and Cu) workpieces were processed with a culture solution of *Acidithiobacillus ferrooxidans* at various jet velocities, and the material removal rate (MRR) was obtained for each metal. The surface topography, roughness, and elements of the workpieces were also measured. The influence of the jet velocity on the MRR was analyzed. The results indicated that the jet velocity significantly influenced the MRR. The maximum MRR was up to 39.7 times that in the shaking mode. A power function relationship exists between the MRR and jet velocity for each metal. The cations participating in a unit of time, pits on the surface, and dissolved oxygen are essential factors

affecting the MRR at various jet velocities. These results will be useful for the development of new methods to improve MRR for effective biomachining.

Keywords: Biomachining; Acidithiobacillus ferrooxidans; Jet velocity; Material removal rate; Roughness.

1. Introduction

Diamond tools are widely used to process hard-brittle materials. The dressing efficiency of diamond tools directly affects the precision machining efficiency of hard-brittle materials, thus impacting the machining cost. Commonly used diamond tool dressing methods include mechanical, electrical discharge, and chemical methods (Ding et al., 2017). Mechanical and electric spark dressing methods inevitably cause surface damage to the diamond (Klink, 2010). Although chemical finishing avoids abrasive wear, it uses several toxic compounds in the grinding fluid (Zhang et al., 2021), resulting in environmental pollution and additional costs. Bioprocessing has become a focus of manufacturing research for cleaner production.

Biomachining has been applied to diamond tool dressings in recent years because it is environmentally friendly and does not cause thermal or mechanical damage (Ma and Huang, 2020). It can continuously remove a metal binder around the abrasive particles with low energy consumption while keeping the abrasive particles intact. During the metal removal process, it produces no heat-affected zones on the workpieces, which causes low environmental pollution (Santaolalla et al., 2023).

Biological machining uses microorganisms to remove metals from a workpiece and includes biomachining, bioforming, and biodeposition (Uno et al., 1996). As an essential branch of biological machining, biomachining has recently been increasingly studied and has been reported as a clean metal processing technology (Pradeep et al., 2022). Several microorganisms, including *A. ferrooxidans (A. ferrooxidans)* (Sonia et al., 2021), *Acidithiobacillus thiooxidans* (*A. thiooxidans*) (Pradeep et al., 2022), *Sulfobacillus thermosulfidooxidans* (*S. thermosulfidooxidans*) (Diaz-Tena et al., 2018) and *Aspergillus niger* (*A. niger*) (Jadhav and Hocheng, 2014), have been used for biomachining metals. Ma et al. (2020) conducted experiments involving the shaking and galvanic corrosion of Cu and Co workpieces using *A. ferrooxidans*. The results revealed a linear relationship between material removal amount (MRA) and processing time when the temperature was 30 °C, and the shaking rate was 160 r/min. They achieved Cu and Co removal rates of 9.27 and 8.53 $mg/cm^2 \cdot h$, respectively. A maximum material removal rate (MRR) of tin (3.5 $mg/cm^2 \cdot h$) was also observed in the experiments with *A. Niger* under the temperature of 30°C at a shaking rate of 150 r/min (Jadhav and Hocheng, 2014). However, a higher corrosion velocity of oxygen-free copper (10.9 $mg/cm^2 \cdot h$) was observed in the application of *A. ferrooxidans* and *S. thermosulfidooxidans* under the agitation conditions of 180 r/min at 30 °C (Diaz-Tena et al., 2014; Diaz-Tena et al., 2018), and a method of the single-stage process was found to shorten the processing time. However, how the agitation conditions alter the corrosion velocity of the workpieces remains unclear.

Furthermore, the shaking rate and other process parameters affect the MRR. An orthogonal test of the shaking removal rate of pure iron was conducted by *A. ferrooxidans* in an incubator shaker with a series of parameters (pH, shaking rate, temperature, and strain concentration in the solution) (Muhammad et al., 2015). The results showed that all the process parameters (except pH) had a direct relationship with the MRR and the shaking rate was one of the critical factors affecting the shaking removal rate. A study on using *A. niger* to remove the tin workpiece showed that the MRR increased rapidly until the shaking rate reached 150 r/min, and the maximum MRR (3.5 mg/ cm^2·h) was observed at 150 r/min, which was the same as that at 200 r/min (Jadhav and Hocheng, 2014). The shaking rate had the most significant impact on the MRR when processing pure copper with *A. ferrooxidans* culture solution. However, the MRR of Cu is limited to shaking rates below 160 r/min. A relatively small enhancement of the Cu MRR was observed when the shaking rate exceeded 160 r/min (Huang and Ma, 2019).

In summary, the shaking rate is one relevant parameter affecting the MRR, and the maximum value is *ca* 10 mg/cm^2·h by shaking. The shaking rate had the most significant effect on the removal efficiency among those process parameters, and the MRR stopped increasing when the shaking rate reached 160 r/min. The low efficiency of biological removal cannot satisfy the demand for rapid binder removal in biological in-process dressings and has become a bottleneck restricting the development of this technology. Therefore, new technologies must be developed to improve biomachining efficiency.

Research on abrasive jet machining (AJM) (Chen et al., 2017) has increased relatively well. The jet velocity reached 1000 m/s (Saravanan et al., 2020). This is much higher than the velocity during biomachining. Unlike biomachining, the removal mechanism of AJM involves collisions with kinetic energy. In the study of AJM, some scholars have found that the jet velocity affects the MRR. A study of the process parameters of AJM observed that the jet pressure, jet velocity, nozzle diameter, and other parameters affect the processing efficiency (Kale et al., 2020). Ravi et al. (2018) compared the parameters of distance, jet velocity, and material ratio during the abrasive water jet processing of carbides. They found that jet velocity influenced the MRR. Therefore, biological jet machining was employed in this study to investigate the effect of jet velocity on jet biomachining processing. In this study, the shaking machining method was transformed into a jet machining method, and the MRA, surface topography, surface roughness (Sa), and surface element distribution of three metal (Fe, Co, and Cu) workpieces were determined after machining at different jet velocities of the biological jet solution.

2. Materials and Methods

In the study, jet-processed Fe, Co, and Cu workpieces were placed on a test platform. A rotary corrosion test was designed to examine the effects of flat fluids.

2.1 Test platform of biomachining experiments

The test platform was designed and built independently before the experiments. As shown in Fig. 1, the test device can be divided into a bacterial circulation culture

system and jet circulation system. The bacterial circulation culture system primarily consisted of a bioreactor, Millipore filter, bidirectional peristaltic pump (NKP-DC-B08B, Kamoer), solution recovery tank, and air pump (SB-988, Sobo), whereas the jet circulation system was primarily composed of a circulating pump (FSZ32×25-11, Minyuan) and solution recovery tank. The solution in the tank was sprayed onto the workpiece using a circulating pump. When the machine was operated, the solution in the splash shield flowed quickly into the solution recovery tank through the holes on the upper and lower covers. The jet velocity was controlled using a stainless-steel ball valve. The solution was extracted using an outlet tube at the bottom of the tank.
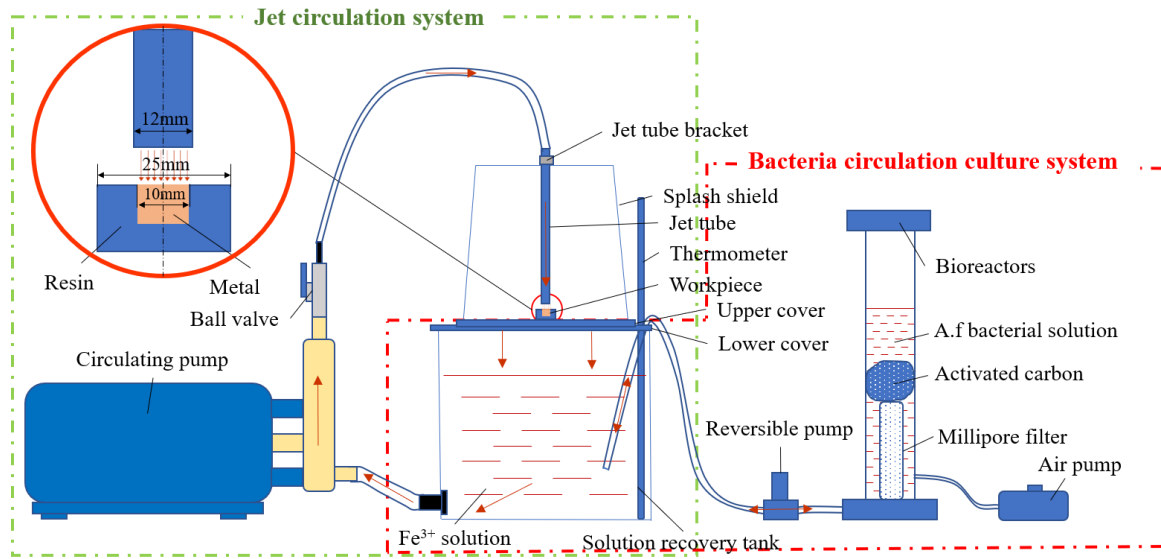
Fig. 1. Schematic of the test platform

The strain of *A. ferrooxidans* used in this experiment was initially provided by the East China University of Technology. The strain was cultured in a 9K medium. The medium consisted of $(NH_4)_2SO_4$ (3 g/L), KCl (0.1 g/L), $K_2HPO_4 \cdot 3H_2O$ (0.5 g/L), $MgSO_4 \cdot 7H_2O$ (0.5 g/L), $Ca(NO_3)_2 \cdot 4H_2O$ (0.01 g/L), and $FeSO_4 \cdot 7H_2O$ (24.8 g/L) (Ma et al., 2020). The seed solution of *A. ferrooxidans* and the medium was mixed at a

volume ratio of 1:4. The pH of the mixed solution was adjusted to 1.8 with 60 % sulfuric acid. Subsequently, the mixed solution was placed into a conical flask and placed in a shaker with the temperature at 30 °C and shaking rate at 160 r/min. During the bacterial culture process, the concentration of Fe^{3+} in the solution was measured using ethylenediaminetetraacetic acid (EDTA) titration (Wu et al., 2003). After 12 h of cultivation, Fe^{2+} in the solution was nearly 100 % converted to Fe^{3+} (Ma et al., 2020), and the culture was terminated. The prepared bacterial solution was then added to the bacterial circulation culture system for the experiments. Subsequently, the bacteria were retained in the bioreactor using the Millipore filter and adsorbed onto the activated carbon package in the bioreactor (Fig. 1). The bioreactor provided a sufficient and continuous bacterial solution for the test platform. The concentrations of the solutions in the bioreactor and solution recovery tank were kept stable by the timing of the bidirectional peristaltic pump.

2.2 Jet experimental method and process parameters

Through vacuum hot pressing sintering at 900°C, the metal wafers of pure Fe, Co, and Cu were prepared with each metal powder of particle size 45 μm. The workpieces were formed with a diameter of 10 mm and thickness of 5 mm and buried in epoxy resin with a diameter of 25 mm and thickness of 8 mm. As shown in Fig. 1, one side surface of the workpiece was exposed; the Sa was polished to about 1 μm; the workpiece was ultrasonic cleaned with alcohol and dried at 60 °C before the test. Subsequently, a 3-h test was conducted, and the samples were weighed at 0, 10, 20, 40,

60, 90, 120, and 180 min. The workpieces were weighed with an electronic balance (FA224, Sunny Hengping) after ultrasonic cleaning with alcohol for 10 min and dried at 60°C for 5 min. The experimental process is shown in Fig. 2.

Fig. 2. Process schematic of jet biomachining experiment

The MRR was calculated using MRA (mg), exposed area S (cm^2), and processing time T (h), as shown in Eq. 1:

$$MRR=MRA/TS \tag{1}$$

where *MRR* is the material removal rate (mg·cm^2·h^{-1}), *MRA* is the material removal amount (mg), *T* is the processing time (h), and *S* is the processing area (2.25 cm^2).

Five jet velocities (0, 1, 2, 3, and 4 m/s) were used in the jet experiments. The workpieces immersed in the solution at a jet velocity of 0 m/s were used as controls. The Reynolds number (Re) of the jet solution was calculated using Eq. 2 (Jiang and Cheng, 2021):

$$Re=\rho vd/\mu \tag{2}$$

where ρ is the fluid density (kg/m^3), v is the fluid velocity (m/s), d is the pipe flow diameter (0.012 m), and μ is the fluid viscosity (Pa·s).

ρ and v can be obtained using Eqs. 3 and 4 (Li et al., 2006):

$$\rho=1.1998-6.3432\times10^{-4}T+26779\times10^{-2}c(H^+)+0.1561c(Fe^{3+}) \tag{3}$$

$$\mu=e^{\wedge}[-5.1775lnT-8.804\times10^{-2}T+1.337\times10^{-4}T^2+8.812\times10^{-2}c(H+)+0.730c(Fe^{3+})] \tag{4}$$

where T is temperature (303 K), $c(H^+)$ is concentration of H^+ (1.59×10^{-2} mol/L), and $c(Fe^{3+})$ is concentration of Fe^{3+} (5 mol/L).

The Re of the fluid ranged from 9866 to 39466 in this experiment. This was greater than 4000, indicating that the jet was turbulent (Chen, 2019). According to the Re and test parameters at different jet velocities, the max boundary layer (δ_{max}) of the jet (0.218 mm) can be calculated using Eqs. 5 and 6 (Pavlovsky, 2020).:

$$\frac{1}{\sqrt{\lambda}}=-2\times lg(\frac{\Delta}{3.7d}+\frac{2.51}{Re\sqrt{\lambda}}) \tag{5}$$

$$\delta_{max}=\frac{32.8d}{Re\sqrt{\lambda}} \tag{6}$$

where λ is the loss factor along the path (m), d is the diameter of the round tube (0.012 m), Δ is pipe roughness (0.01mm), and δ_{max} is the max boundary layer (mm).

The δ_{max} of the jet was 0.218 mm. The diameter of the cylindrical nozzle using in the experiments was 12 mm. The workpiece size was 10 mm, and it was located at the center of the jet impingement zone. Therefore, the solution velocity could be considered to be the actual jet velocity.

Before and after machining, the proportion of the surface elements of the workpieces and surface photos were obtained using a built-in energy spectrometer benchtop scanning electron microscope (Phenom ProX, Phenom-World). The oxygen atom content was expressed as a percentage of the number of oxygen atoms in the visual field relative to the sum of the oxygen and metal atoms. The roughness was detected

using a laser confocal microscope (LSM700, Zeiss) in a sampling area of 0.66 × 0.66 mm^2.

2.3 Rotary machining test

Rotary corrosion tests were conducted using a rotary machining device. As shown in Fig. 3, the workpiece was fixed at the end of the rotating shaft of the motor. The MRRs corresponding to different jet velocities were obtained using different linear speeds on the rotating end face. A mixer (VRera JJ-1) was used in the experiment to perform the rotary-machining test at a rate of 3000 r/min and a test time of 3 h. Before machining, the workpiece surface was polished to a roughness of 90 nm and completely immersed in the bacterial solution (Fig. 3).
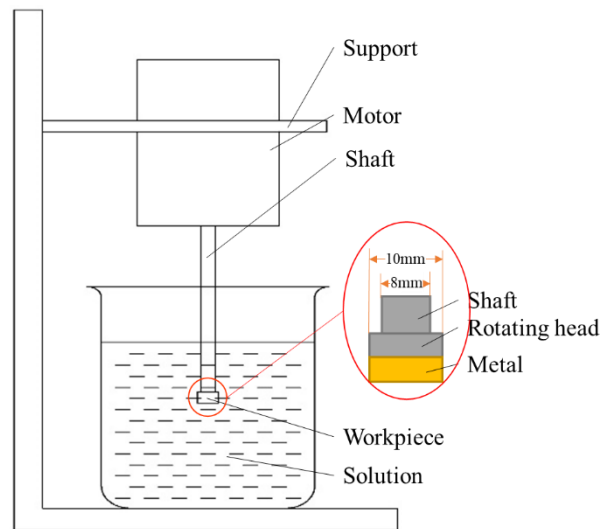
Fig. 3. Rotary machining device

The radial height of the rotating corrosion surface was measured using a laser displacement sensor (LK-G150, Keyence).

3. Results

The results are summarized from three aspects: the effect of jet velocity on MRA, the surface topography, and the impact of jet velocity on Sa.

3.1 Effect of jet velocity on MRA of different metals

Fig. 4 shows the change in MRA over time after the three tests. When the solution was static, the MRAs of all three metal workpieces were approximately 0 mg/cm^2. All the MRAs increased linearly with the jet velocity, and the processing time was extended; however, the changes in the MRAs differed among the three metal workpieces (Fig. 4). The largest MRA was observed for Fe and the smallest for Cu. After 3 h of machining at 4 m/s, the MRAs of Fe, Co, and Cu were 674.24, 390.38, and 277.31 mg/cm^2, respectively. The MRA of Fe was 1.73 times higher than that of Co and 2.43 times higher than that of Cu.
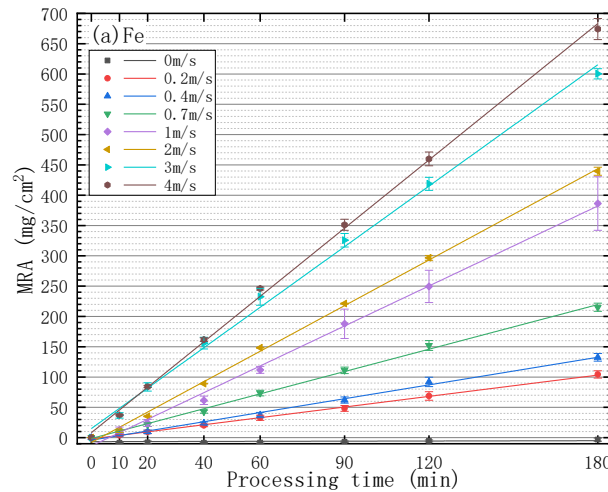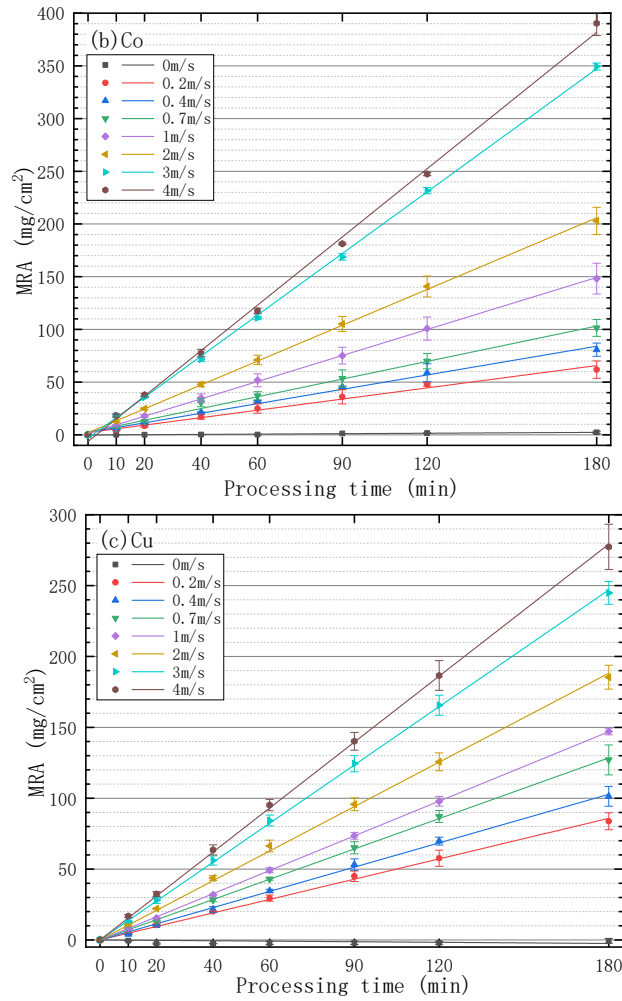
Fig. 4. MRA of (a) Fe, (b) Co, and (c) Cu workpieces with the processing time at different jet velocities

3.2 Surface topography of different metal workpieces processed at different jet velocities

Fig. 5 shows the surface topography of the Fe, Co, and Cu workpieces processed at different jet velocities. Polished scratches were clearly visible on the initially polished surface (Fig. 5a1, 5b1, and 5c1). After 3 h of processing, the scratches on the surface of the Fe workpiece almost disappeared at a jet velocity of 0 m/s, but those on the surface of the Co workpiece were still observed (Fig. 5a2 and 5b2). Although

scratches were also observed on the Cu surface, they were not as clear (Fig. 5c2). At a jet velocity of 1 m/s, erosion pits were apparent on the surfaces of Fe and Cu, particularly on the surface of Fe (Fig. 5a3 and 5c3). The initial polishing marks disappeared for Co, and the surface was large and flat with only a few small pits (Fig. 5b3). When the jet velocity was increased to or higher than 2 m/s, the surface topographies of Fe and Cu did not significantly change according to their color distributions (Fig. 5a4-6 and 5c4-6). However, the surface topography of Co exhibited a large difference from that at a jet velocity of 1 m/s. Many pits appeared on the surface of the Co workpiece (Fig. 5b4-6).
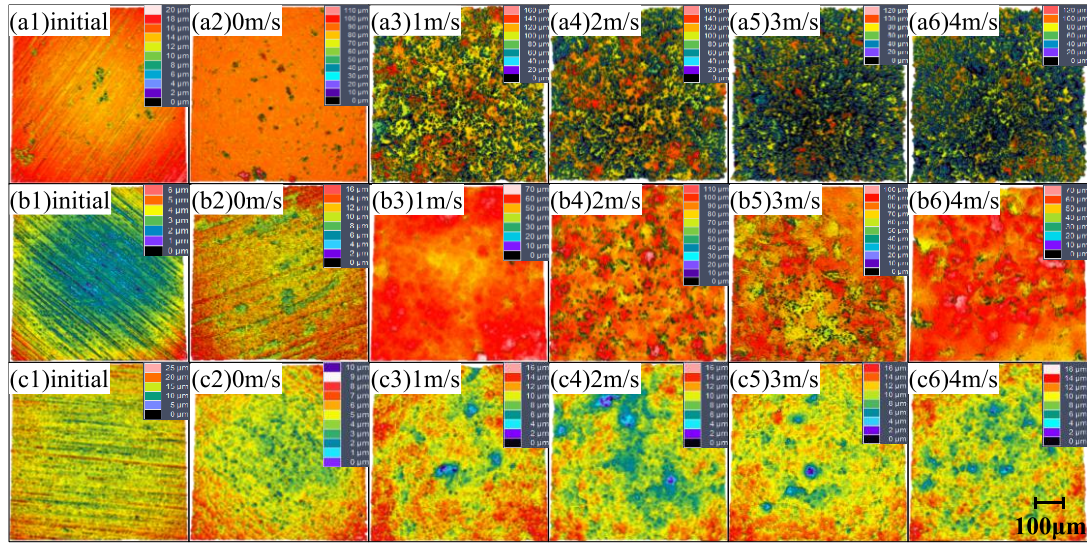
Fig. 5. Surface topography of (a) Fe, (b) Co, and (c) Cu workpieces after 3 h biomachining at different jet velocities

Fig. 6 shows the electron micrographs of the workpiece surface before and after machining. The apparent transition points of the three metal workpieces' topography in (Fig. 6a2-3), (Fig. 6b3-4), and (Fig. 6c2-3) matched well with Fig.5. As shown in the photographs, the three metal workpieces retained many polished surfaces at 0 m/s.

When the flow rate reached 1 m/s, the Fe and Cu surfaces began to form pits. The surface of Fe had many large pits, whereas the surface of Cu has few small pits. The topography of Co changed at 2 m/s, and noticeable corrosion pits appeared.
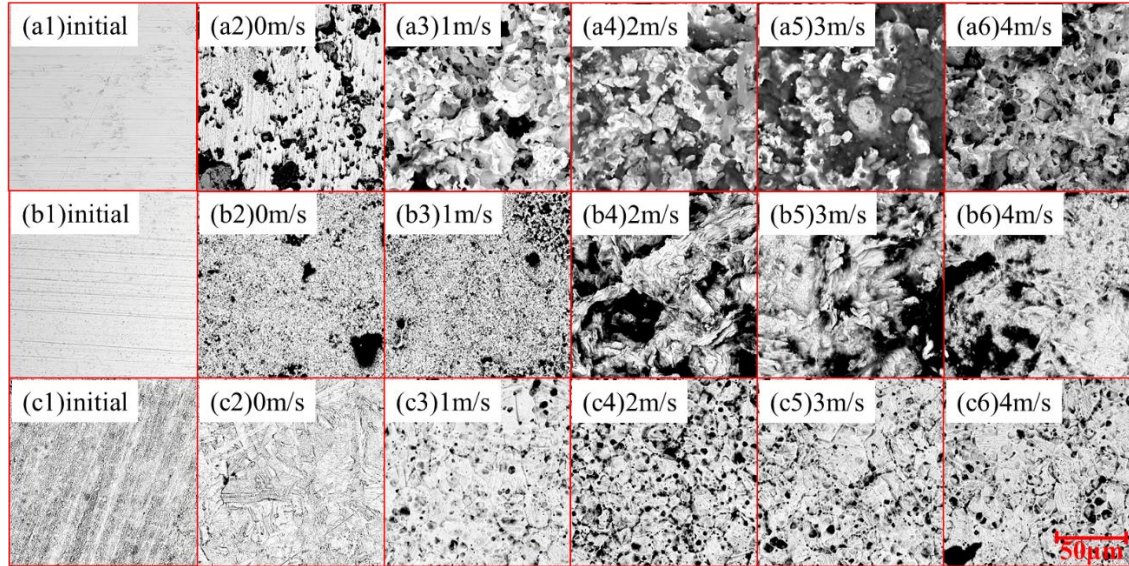

Fig. 6. Surface photos of (a) Fe, (b) Co, and (c) Cu workpieces after 3 h biomachining at different jet velocities

3.3 Effect of jet velocity on Sa of different metal workpieces

Fig. 7 shows the Sa values of the three metal workpieces before and after machining. At a jet velocity of 0 m/s, the Sa values of the three metal workpieces (Fe, Co, and Cu) were similar to those in the initial state. However, the Sa rapidly increased with the jet velocity, and the Sa of all three metal workpieces peaked at 2 m/s with 18.52 μm for Fe, 6.39 μm for Co, and 1.64 μm for Cu. The Sa values of Fe and Co increased significantly after processing with the jet solution, but that of Cu increased more gradually than those of Fe and Co. Similarly, the Sa values of Fe, Co, and Cu decreased slightly with a further increase in the jet velocity. The Sa of the three metal workpieces

14

after the machining process were ranked in the following order: Fe > Co > Cu. This was consistent with the topographies shown in Figs. 5 and 6.
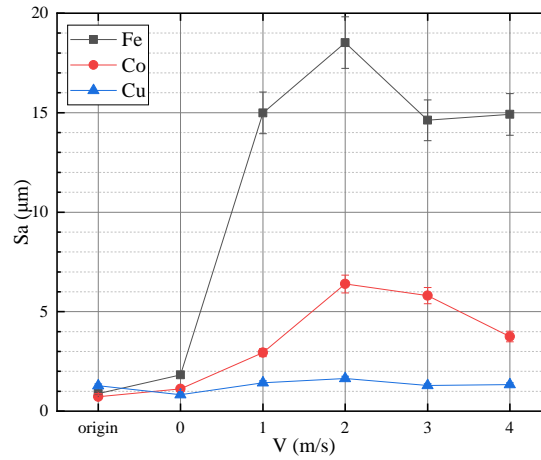

Fig. 7. Surface roughness (Sa) of Fe, Co, and Cu workpieces processed at different jet velocities (V)

4. Discussion

In this study, jet machining was applied to the metal workpieces with the solution of *A. ferrooxidans*; all the MRRs of Fe, Co, and Cu increased significantly with the increase in jet velocity, and extremely high MRRs of the three metal workpieces were obtained at the jet velocity of 4 m/s: the MRRs of Fe, Co, and Cu were 224, 130, and 93 mg/cm^2·h, respectively (Fig. 8). The results for Fe, Co, and Cu were 39.7, 22.0, and 12.5 times, respectively, as high as those reported by Ma et al. (2020). Such a high MRR has not been previously reported for biomachining with *A. ferrooxidans*. This indicated that new strategies to shorten the time required for metal biomachining using a jet can be developed.
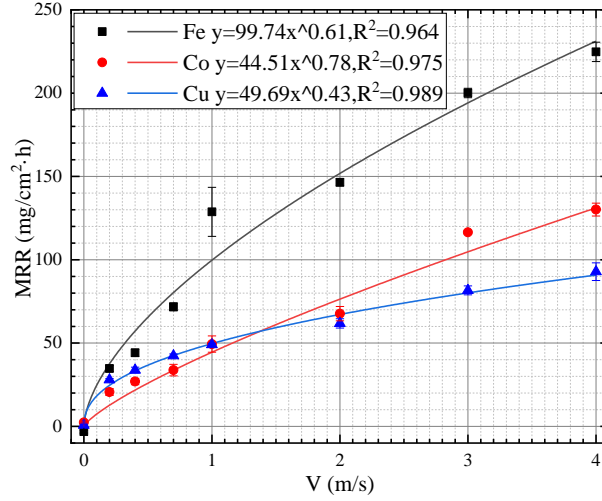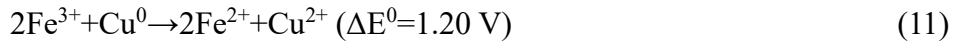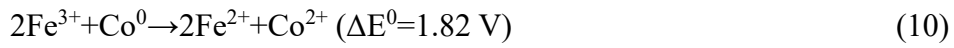
Fig. 8. Relationships between MRR and jet velocity (V) for metal workpieces respectively

As is well known, Fe^{2+} can be rapidly converted to Fe^{3+} in the metabolism process of *A. ferrooxidans*. The principle of biomachining for metal materials is based on the conversion of Fe^{2+} to Fe^{3+} in bacterial solutions (Kang and Wang, 2022). In contrast, the Fe^{3+} in solution can oxidize metals into metal cations. Meanwhile, Fe^{3+} is reduced to Fe^{2+}, and the newly generated Fe^{2+} is returned to the metabolic processes of *A. ferrooxidans*. The biomachining reaction process is shown in Eqs. 7 and 8 (Ma et al., 2020).

$$Fe^{2+} \xrightarrow{A.\ ferrooxidans} Fe^{3+} + e^- \tag{7}$$

$$nFe^{3+} + M \rightarrow nFe^{2+} + M^{n+} \tag{8}$$

In the jet experiments, the MRRs of Fe, Co, and Cu differed under the same machining parameters (Fig. 8), which could be explained by the nature of the metals. The electrode potentials of various metals are different, and the standard potential difference of the reaction (ΔE^0) represents the potential of the reaction trends. Generally,

16

the larger the ΔE^0 is, the faster the reaction will proceed (Ge and Isgor, 2007). According to the ΔE^0 of the reaction between Fe^{3+} and the metals, their order is Fe (1.21 V) > Co (1.05 V) > Cu (0.43 V). We can deduce that the reaction rate in the biomachining process is in the order Fe > Co > Cu under the same conditions. Thus, the MRR performance for the three metal workpieces is in the order Fe > Co > Cu, as calculated in Eqs. 9, 10, and 11.

$$2Fe^{3+}+Fe^0 \rightarrow 3Fe^{2+} \ (\Delta E^0 = 1.98 \ V) \tag{9}$$

$$2Fe^{3+}+Co^0 \rightarrow 2Fe^{2+}+Co^{2+} \ (\Delta E^0 = 1.82 \ V) \tag{10}$$

$$2Fe^{3+}+Cu^0 \rightarrow 2Fe^{2+}+Cu^{2+} \ (\Delta E^0 = 1.20 \ V) \tag{11}$$

According to the molecular collision theory, the root of the reaction is molecular collisions. The mechanism for accelerating the MRR of *A. ferrooxidans* involves intensifying the collisions between the solid metal and Fe^{3+} in the culture solution, and the intensity of the collision directly affects the efficiency of biological processing. This was confirmed by the shaking experiments conducted by Jadhav et al. (2014), who concluded that an increased shaking rate would effectively improve the MRR. In contrast, in this experiment, the jet action on the metal surface caused violent liquid motion, as shown in Fig. 9, which resulted in an intensified collision between the molecules. In this case, the number of ions involved in the reaction per unit time determined the reaction rate of electrochemical corrosion and thus affected the MRR. Therefore, the higher the jet velocity, the larger the number of particle collisions that occur, and a larger MRR is expected. This can be explained by practical collision theory (Someda, 2017), which indicates that chemical reactions have a fixed average reaction

rate under fixed reaction conditions, and the reaction rate is the effective collision quantity per unit volume per unit of time. Therefore, the concentration of Fe3+ and the jet velocity affect the MRR to some extent. Of course, the MRR will not increase without limit with jet velocity; the volume of the reaction site and the chemical reaction rate have upper limits, which may depend primarily on the properties of the metals.
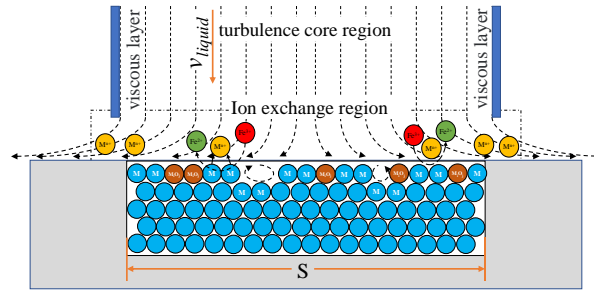

Fig. 9. Schematic of flow state and ion conversion in jet biomachining area

Furthermore, note that the relationship between the MRR and jet velocity is not linear but a power function with a coefficient of determination (R^2) above 96 % for all three metal workpieces. The jet velocity required to obtain the target MRR can be estimated using this function, which can then be used as a reference for controlling the jet biomachining rate. The nonlinear relationship indicates that the MRR does not increase indefinitely with the jet velocity. Other factors hinder the increase in the MRR. The linear relationship between the MRA and processing time shown in Fig. 4 indicates that the MRR is constant when the jet velocity is constant, as confirmed by the results of Ma et al. (2020). The growth rate of the MRR gradually decreased with an increase in jet velocity. A similar phenomenon was also observed in studies by Zhao et al. (2022), Li et al. (2020), and Zhao et al. (2008). Zhao et al. explained that the corrosion rate of a corroded surface is controlled by a combination of the electrochemical reaction rate

and the rate of diffusion and that the diffusion rate is not linearly related to the jet velocity. The results confirmed that the pits on the workpiece surface become more evident with an increase in jet velocity (Fig. 5), which was consistent with the results of Zhao et al. (2008).

When comparing the MRRs under the same biomachining conditions, Fe always had a higher MRR than the other two metals. Co had a lower MRR than Cu at a low velocity (1 m/s). However, its MRR increased rapidly and exceeded that of Cu with increasing jet velocity (Fig. 8). The change in the MRR was consistent with the topography change shown in Fig. 5. When the solution was static, residual scratches were apparent on the Co surface; however, fewer scratches were observed on the Cu surface. When the jet velocity was 1 m/s, the Co surface was relatively flat, whereas a few pits appeared on the surface of Cu (Zhang et al., 2022). Thus, the pits on the surface of the workpieces increased the reaction area. With an increase in velocity, many pits appeared on the surface of the Co workpiece, but the results were different for the Cu workpiece. Therefore, the MRR of Co began to exceed that of Cu when the velocity exceeded 2 m/s (Fig. 8). This could be related to the material properties of Cu (Xu et al., 2021). In the machining process, no significant number of erosion pits were produced to form a loose layer on the surface of Cu.

Some researchers have reported that dissolved oxygen is involved in the oxidation of metals in solution (Mahmood et al., 2017). As shown in Fig. 10, although the proportion of oxygen atoms on the surface of each metal fluctuated significantly with the jet velocity, the value increased to a certain extent after machining. The stability of

the oxides formed on metal surfaces hindered their removal (Mahmood et al., 2017).

As shown in Fig. 10, in the initial state, the proportion of oxygen on the metal surface

decreased in the order of Fe (15.5 %) > Co (12.4 %) > Cu (11.0 %). After machining,

the maximum number of oxygen atoms observed in the experiments differed among the

metals. Fe and Co had a maximum oxygen ratio at 4 m/s; the highest value of Fe (36.7 %)

was 2.37 times higher than that in the initial state, and the value of Co (24.2 %) was

1.95 times higher than that in the initial state. Cu reached its maximum value at 2 m/s

(22.9 %), which was 2.08 times higher than that in the initial state. This demonstrated

that the highest proportion of oxygen atoms on the surface of the workpiece, from

highest to lowest was Fe >Co > Cu, which agreed with the order of MRA and MRR.
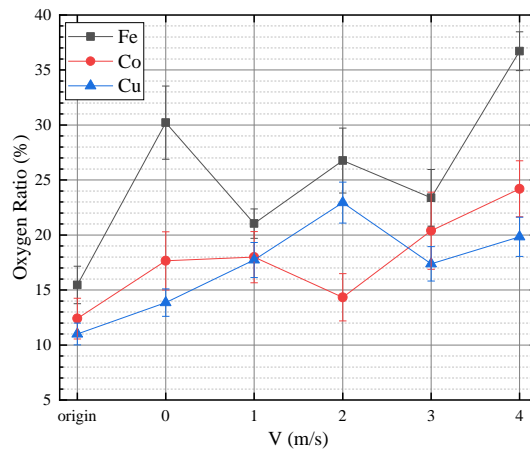
Fig. 10. Oxygen ratios changing with the jet velocity (V) of solution

These jet experiments showed that an increase in the jet velocity significantly

affects the MRR. However, note that the MRR did not increase significantly in earlier

experiments with shaking rates higher than 160 r/min. The removal heights of the

workpiece along the radial direction after 3 h of rotary machining are shown in Fig. 11

(experimental curve), where the zero point of the X-axis is the center of the workpiece. The removal height (*Y*-calculated) is calculated using Eq. 12:

$$Y=10^4 \times MRR \times T/\rho \qquad (12)$$

where *Y* is the removal height (μm), *T* is the processing time (h), ρ is the metal density (mg/cm^3), and *MRR* is the material removal rate calculated from the fitting formula in Fig. 7 (mg/cm^2·h).

Under rotational machining conditions, the angular velocities of the different reaction sites on the workpiece were the same; however, the linear velocity increased as the radius increased. However, the actual removal curve was significantly different from the curve fitted using the above formula (Fig. 11). This suggests that the effects of the material removal generated by the jet on the workpiece are different from the movement of the metal immersed in the fluid at the same velocity. Aouinet et al. (2021) indicated the existence of a boundary layer on the plate's surface in the liquid, and the velocity near the surface is close to zero. Therefore, in the rotation experiment, the velocity distribution on the workpiece surface differed significantly from that of the rotated workpiece. Thus, the experiment did not successfully fit or achieve the expected effects. Similarly, no slip occurred between the walls during the shaking biomachining. This implied that the actual fluid velocity involved in machining was significantly lower than the preset fluid velocity. Therefore, biomachining removal efficiency was low in other studies (Hemalatha et al., 2021; Sonia et al., 2021). Therefore, the MRRs of all previous scholars have been significantly limited in shaking biomachining.
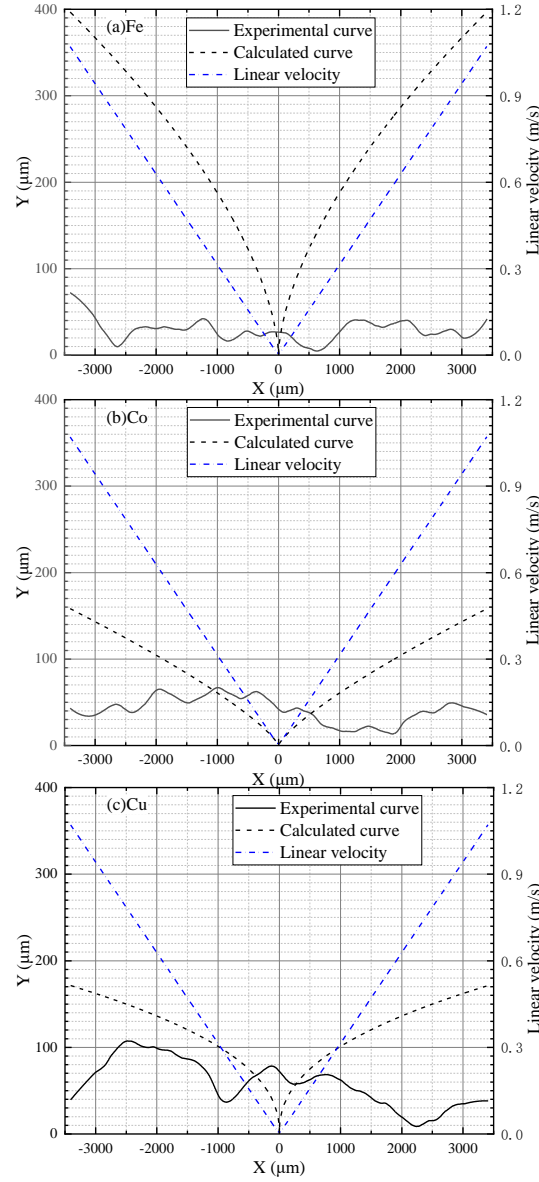
Fig. 11. Removal heights of (a) Fe, (b) Co, and (c) Cu workpieces along the radial direction after 3 h of rotary machining

5. Conclusion

This study analyzed the effect of jet velocity on the efficiency of biomachining metals. The effects of the jet velocity, surface topography, surface roughness, and surface elements are discussed. The conclusions are summarized below.

(1) The MRR improved with jet velocity. The maximum MRRs of jet biomachining of Fe, Cu, and Co reached 224, 130, and 93 mg/cm^2·h at 4 m/s, which are 39.7, 22.0, and 12.5 times higher than that in shaking biomachining, respectively.

(2) A power function relationship exists between the MRR and jet velocity, with a coefficient of determination (R^2) above 96 % for all three metal workpieces.

(3) The surface roughnesses of Fe, Co, and Cu fluctuate around 15.8, 5.3, and 1.2 μm after jet biomachining, respectively.

(4) The MRR with jet biomachining was a combined effect of the cations participating in the unit time, pits on the surface, metal oxides generated on the surface, and dissolved oxygen.

Acknowledgments

References:

Aouinet, H., Dhahri, M., Safaei, M.R., Sammouda, H., Anqi, A.E., 2021, Turbulent boundary layers and hydrodynamic flow analysis of nanofluids over a plate. J Cent South Univ 28, 3340-3353.http://dx.doi.org/10.1007/s11771-021-4859-7

Chen, F., Miao, X., Tang, Y., Yin, S., 2017, A review on recent advances in machining methods based on abrasive jet polishing (AJP). Int J Adv Manuf Tech 90, 785–799.http://dx.doi.org/10.1007/s00170-016-9405-7

Chen, X.D., 2019, Laminar-to-Turbulence Transition Revealed Through a Reynolds Number Equivalence. Eng 5, 576–579.http://dx.doi.org/10.1016/j.eng.2018.09.013

Diaz-Tena, E., Gallastegui, G., Hipperdinger, M., Donati, E.R., Rojo, N., Santaolalla, A., Ramirez, M.,

Barona, A., Elías, A., 2018, Simultaneous Culture and Biomachining of Copper in MAC Medium: A Comparison between Acidithiobacillus ferrooxidans and Sulfobacillus thermosulfidooxidans. Acs Sustain Chem Eng 6, 17026–17034.http://dx.doi.org/10.1021/acssuschemeng.8b04348

Diaz-Tena, E., Rodríguez-Ezquerro, A., López De Lacalle Marcaide, L.N., Gurtubay Bustinduy, L., Elías Sáenz, A., 2014, A sustainable process for material removal on pure copper by use of extremophile bacteria. J Clean Prod 84, 752–760.http://dx.doi.org/10.1016/j.jclepro.2014.01.061

Ding, W., Li, H., Zhang, L., Xu, J., Fu, Y., Su, H., 2017, Diamond Wheel Dressing: A Comprehensive Review. J Manuf Sci Eng 139, 121006. https://doi.org/10.1115/1.4037991

Ge, J., Isgor, O.B., 2007, Effects of Tafel slope, exchange current density and electrode potential on the corrosion of steel in concrete. Mater Corros 58, 573-582.http://dx.doi.org/10.1002/maco.200604043

Hemalatha, B., Rajeswari, B., Sekar, T., Rajasekar, V., 2021. Experimental Studies on Biomachining of Copper and Its Behavioural Characteristics. In: Mohan, S., Shankar, S., Rajeshkumar, G. (Eds.), Springer Singapore, Singapore, pp. 49-56. http://dx.doi.org/10.1007/978-981-15-9809-8_4

Huang, H., Ma, F., 2019, Parameter Optimization for Improvement in Biomachining Performance. Trans Nanjing Univ Aeronaut Astronaut 36, 376–386.http://dx.doi.org/10.16356/j.1005

Jadhav, U., Hocheng, H., 2014, Use of Aspergillus niger 34770 culture supernatant for tin metal removal. Corros Sci 82, 248-254.http://dx.doi.org/10.1016/j.corsci.2014.01.011

Jiang, H., Cheng, L., 2021, Large-eddy simulation of flow past a circular cylinder for Reynolds numbers 400 to 3900. Phys Fluids 33.http://dx.doi.org/10.1063/5.0041168

Kale, A., S. K., S., N., S., Subbiah, R., 2020, A review on abrasive water jet machining process and its process parameters. Mater Today 26, 1032-1036.http://dx.doi.org/10.1016/j.matpr.2020.01.309

Kang, J., Wang, Y., 2022, The role of Acidithiobacillus ferrooxidans in Fe(II) oxidation of pyrite in bioleaching processes. J Chem Tech Biotechnol 97, 2013-2023. https://doi.org/10.1002/jctb.7072

Klink, A., 2010, Wire electro discharge trueing and dressing of fine grinding wheels. CIRP Annals 59, 235–238.http://dx.doi.org/10.1016/j.cirp.2010.03.076

Li, F., Li, Y., Cao, Z., Wang, W., Liang, F., Zhang, H., 2006, Measurement of densities and viscosities for mixed solutions of FeSO4-Fe2(SO4)3-H2SO4. Chem Eng, 39–42.https://kns.cnki.net/kcms/detail/detail.aspx?FileName=IMIY200604010&DbName=CJFQ2006

Li, Y., Liu, D., Zhu, G., Zhang, G., 2020, Effects of Temperature and Flow Velocity on the Corrosion Behavior of N80 Carbon Steel in Supercritical CO2 Environment. Surf Tech 49, 35–41.http://dx.doi.org/10.16490/j.cnki.issn.1001-3660.2020.03.005

Ma, F., Huang, H., 2020, Experimental research on the biological in-process dressing (BID) of Cu−Co matrix diamond tools. J Clean Prod 275, 124070.http://dx.doi.org/10.1016/j.jclepro.2020.124070

Ma, F., Huang, H., Cui, C., 2020, Biomachining properties of various metals by microorganisms. J Mater Process Tech 278, 116512.http://dx.doi.org/10.1016/j.jmatprotec.2019.116512

Ma, F., Huang, H., Xu, X., 2020, Material Removal Mechanisms of Cu‐Co Metal-Powder Composite by Microorganisms. Int J Pr Eng Man-Gt 7, 975-986.http://dx.doi.org/10.1007/s40684-019-00110-8

Mahmood, M.H., Suryanto, Al Hazza, M.H., 2017. The effects of water flow rate on copper corrosion. Trans Tech Publications Ltd, Singapore, Singapore, pp. 235–239. http://dx.doi.org/10.4028/www.scientific.net/KEM.748.235

Muhammad, I., Sana Ullah, S.M., Han, D.S., Ko, T.J., 2015, Selection of optimum process parameters of biomachining for maximum metal removal rate. Int J Pr Eng Man-Gt 2, 307-313.http://dx.doi.org/10.1007/s40684-015-0037-4

Pavlovsky, V.A., 2020, Analysis of steady flow in a circular cylindrical pipe with hydraulically smooth walls. Marine Intellectual Tech 2, 93–98.http://dx.doi.org/DOI 10.37220/MIT.2020.48.2.051

Pradeep, M., Rajesh, S., Uthayakumar, M., Sivaranjana, P., Syath Abuthakeer, S., Ravichandran, M., Thiagamani, S.M.K., Mavinkere Rangappa, S., Siengchin, S., 2022, Investigations on the combined effects of Thiobacillus Novellus microorganism and process parameters on the bio-machining of NiTi. Biomass Cinvers Bior.http://dx.doi.org/10.1007/s13399-022-03616-5

Pradeep, M., Shanmugavel, R., Uthayakumar, M., Muthulakshmi, L., Adam Khan, M., Thiagamani, S.M.K., Rangappa, S.M., Siengchin, S., 2022, Experimental studies on biomachining process using novel Thiobacillus novellus microorganism-a comparative study. Biomass Convers Bior.http://dx.doi.org/10.1007/s13399-022-03189-3

Ravi, K.K., Sreebalaji, V.S., Pridhar, T., 2018, Characterization and optimization of Abrasive Water Jet Machining parameters of aluminium/tungsten carbide composites. Meas 117, 57–66.http://dx.doi.org/10.1016/j.measurement.2017.11.059

Santaolalla, A., Alvarez-Brana, Y., Barona, A., Basabe-Desmonts, L., Benito-Lopez, F., Rojo, N., 2023, Sustainable mold biomachining for the manufacturing of microfluidic devices. J Ind Eng Chem 120, 332–339.http://dx.doi.org/10.1016/j.jiec.2022.12.040

Saravanan, S., Vijayan, V., Suthahar, S.T.J., Balan, A.V., Sankar, S., Ravichandran, M., 2020, A review on recent progresses in machining methods based on abrasive water jet machining. Mater Today: Proc 21, 116–122.http://dx.doi.org/10.1016/j.matpr.2019.05.373

Someda, K., 2017, Standard deviations of chemical reaction rates and validity ranges of the statistical theory. Mol Phys 115, 2389-2404.http://dx.doi.org/10.1080/00268976.2017.1320435

Sonia, Sodhi, A.K., Bhanot, N., 2021. Biomachining of Aluminum Alloy 46500 Using Acidithiobacillus ferrooxidans., Springer Science and Business Media Deutschland GmbH, Ludhiana, India, pp. 567–579. http://dx.doi.org/10.1007/978-981-15-9554-7_51

Uno, Y., Kaneeda, T., Yokomizo, S., 1996, Fundamental study on biomachining : Machining of metals by thiobacillus ferrooxidans. JSME international journal. Series C, Dynamics, control, robotics, design and manufacturing 39, 837–842.http://dx.doi.org/10.1299/jsmec1993.39.837

Wu, L.H., Luo, Y.M., Christie, P., Wong, M.H., 2003, Effects of EDTA and low molecular weight organic acids on soil solution properties of a heavy metal polluted soil. Chemosphere 50, 819–822. http://dx.doi.org/10.1016/s0045-6535(02)00225-4

Xu, H., Song, E., Bian, D., Zhao, Y., 2021, Investigation of weak corrosion inhibitor for copper chemical mechanical polishing. Diam Abras Eng 41, 32-39.http://dx.doi.org/10.13394/j.cnki.jgszz.2021.5.0006

Zhang, P., Yang, X., Chen, B., Huang, L., Pian, X., Li, Z., Yan, N., Wang, X., Sun, G., Zhang, P., Li, Z., Ci, Z., Chen, Q., Yi, J., Li, J., 2022, Effect of room temperature cobalt removal on the microstructure and mechanical properties of PCD. Diam Abras Eng 42, 685-691.http://dx.doi.org/10.13394/j.cnki.jgszz.2022.0052

Zhang, Z., Liu, J., Hu, W., Zhang, L., Xie, W., Liao, L., 2021, Chemical mechanical polishing for sapphire wafers using a developed slurry. J Manuf Process 62, 762–771.http://dx.doi.org/10.1016/j.jmapro.2021.01.004

Zhao, G., Lv, X., Han, Y., 2008, Effect of Flow Rate on CO2 Corrosion Behavior of P110 Steel. J Mater Eng, 5–8. https://kns.cnki.net/kcms/detail/detail.aspx?FileName=CLGC200808001&DbName=CJFQ2008

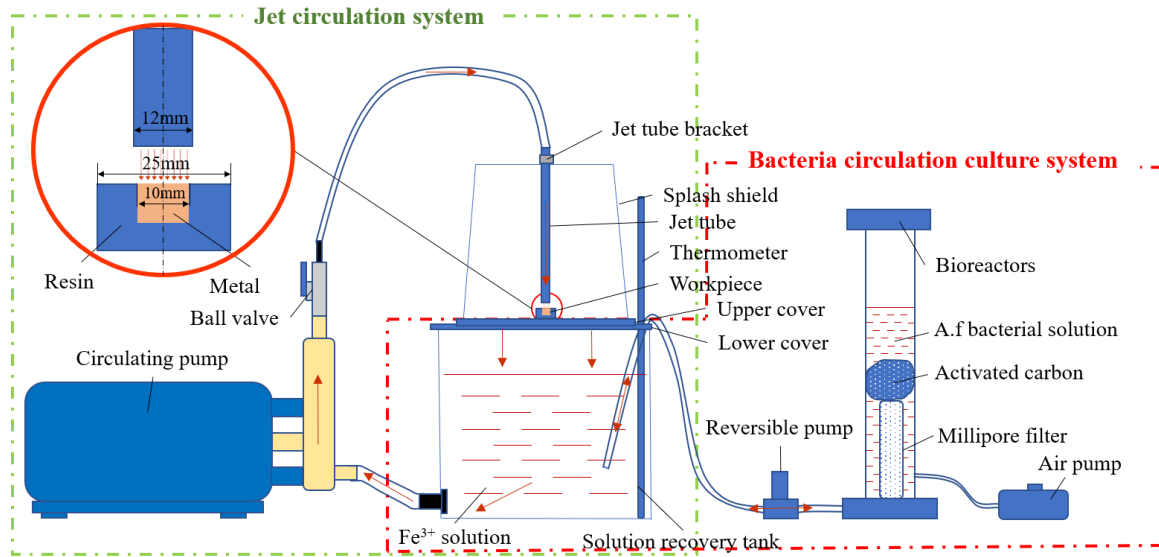Zhao, S., Liao, K., He, G., Leng, J., Qin, M., Zou, Q., Pang, H., 2022, Study on the Corrosion Behavior

of L320 Steel at Different Flow Rates in CO2/O2 Enviroment. Mater Prot 55, 95–101.http://dx.doi.org/10.16577/j.issn.1001-560.2022.0011

Fig. 1. Schematic of the test platform

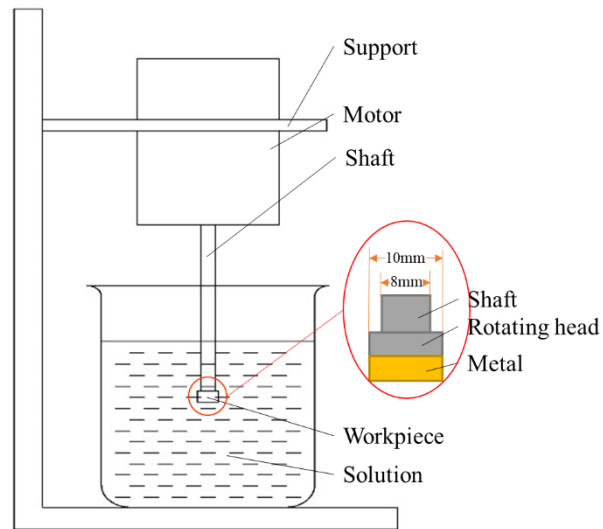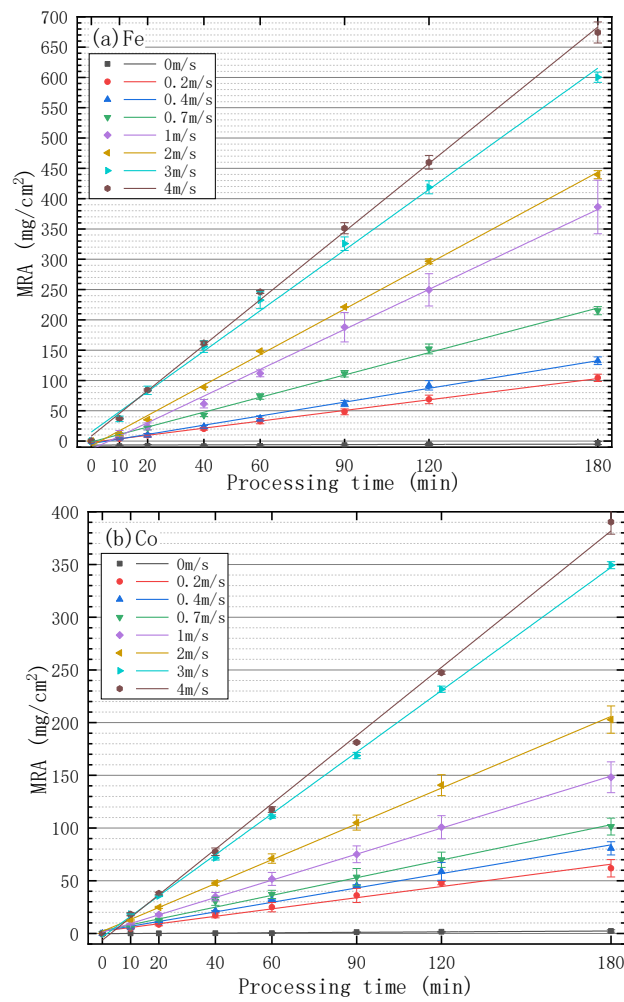**Fig. 2.** Process schematic of jet biomachining experiment
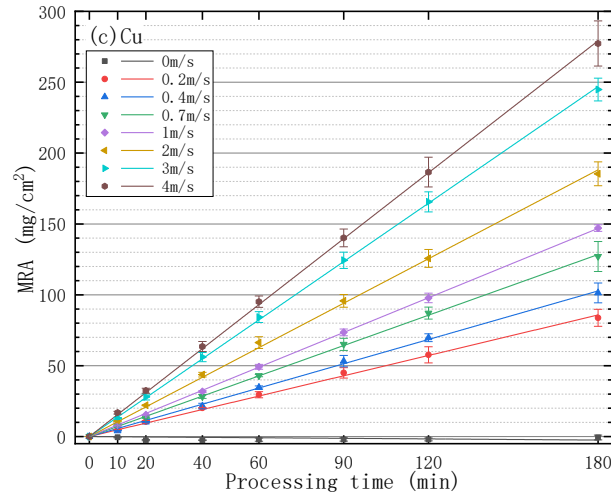
Fig. 3. Rotary machining device

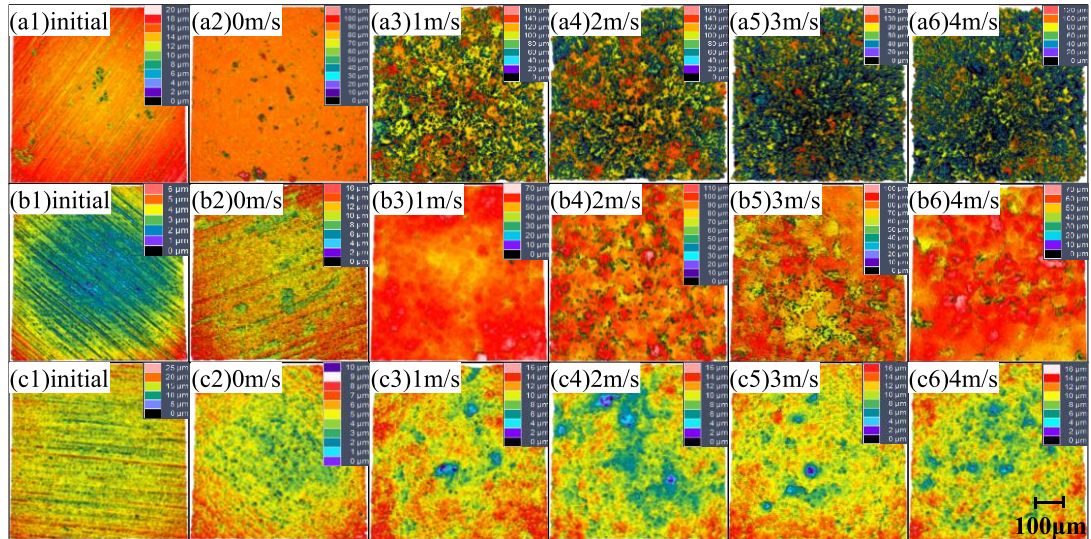**Fig. 4.** MRA of (a) Fe, (b) Co, and (c) Cu workpieces with the processing time at different jet velocities

Fig. 5. Surface topography of (a) Fe, (b) Co, and (c) Cu workpieces after 3 h biomachining at different jet velocities
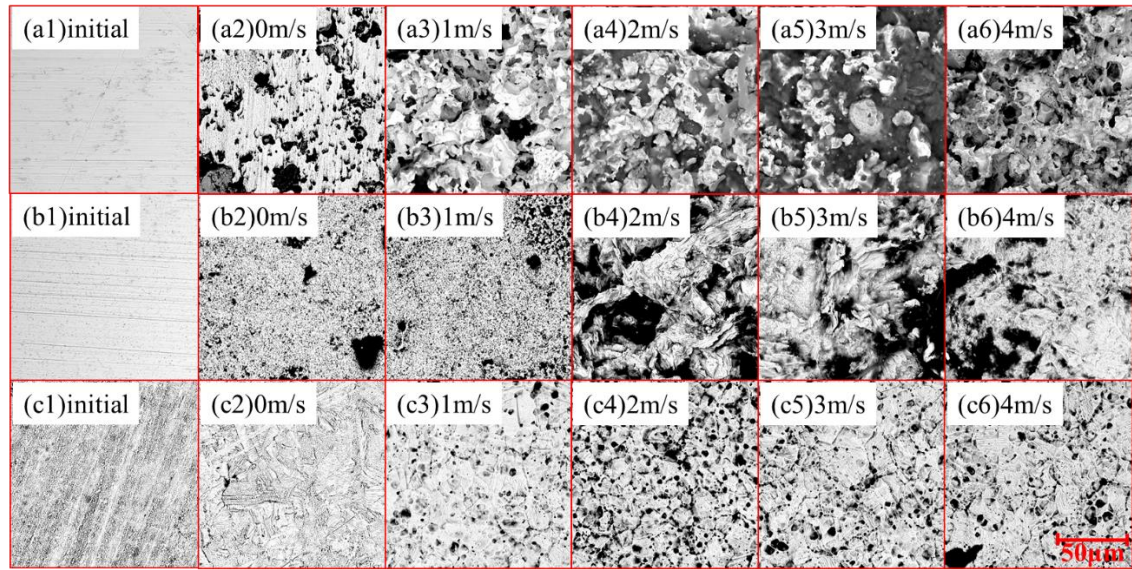
Fig. 6. Surface photos of (a) Fe, (b) Co, and (c) Cu workpieces after 3 h biomachining

at different jet velocities
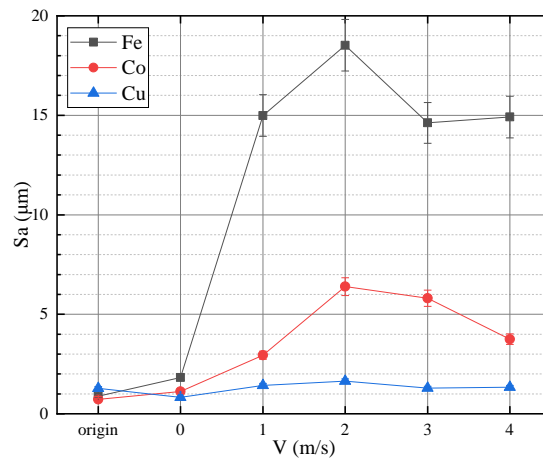
Fig. 7. Surface roughness (Sa) of Fe, Co, and Cu workpieces processed at different jet

velocities (V)
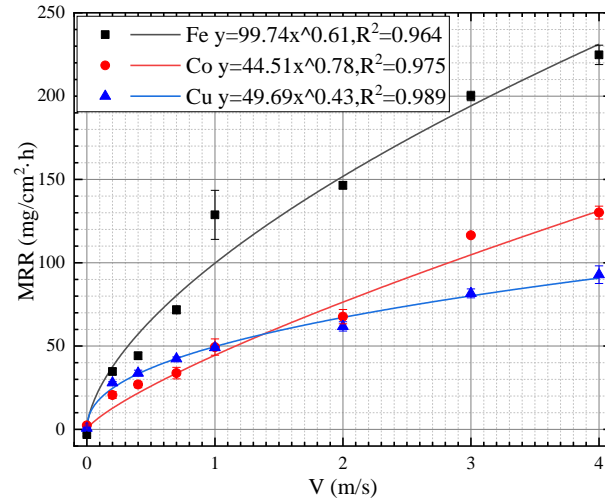
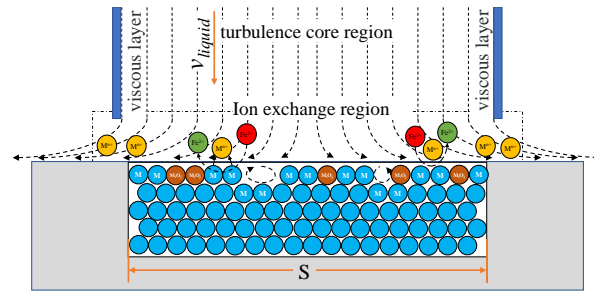**Fig. 8.** Relationships between MRR and jet velocity (V) for metal workpieces respectively

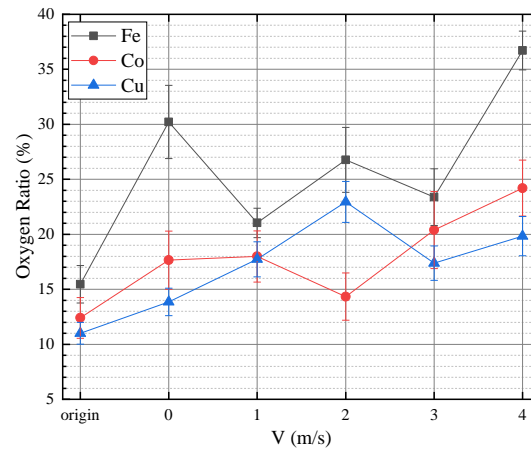**Fig. 9.** Schematic of flow state and ion conversion in jet biomachining area

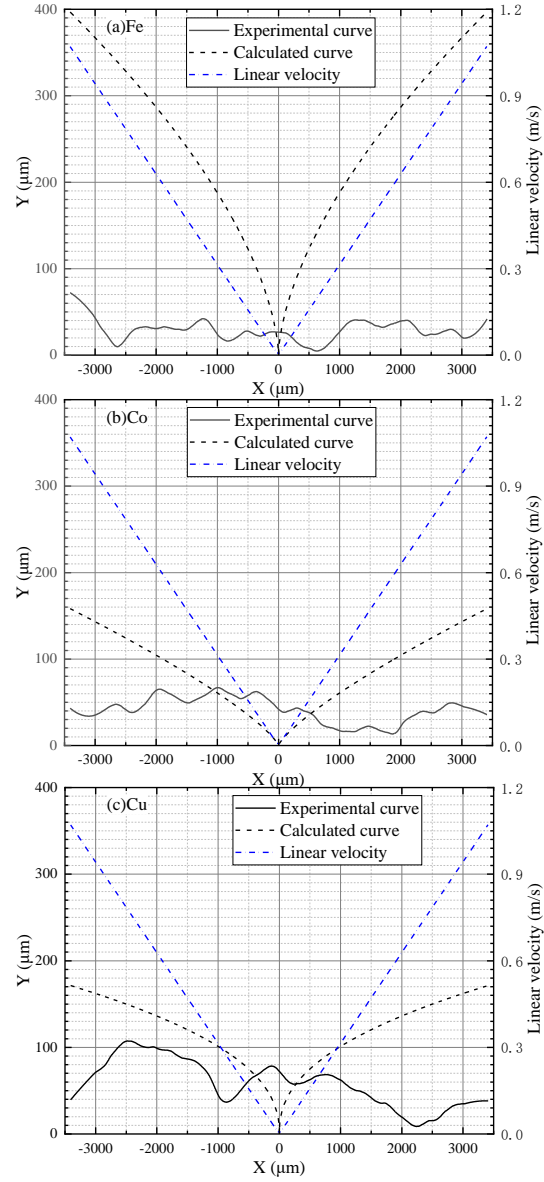**Fig. 10.** Oxygen ratios changing with the jet velocity (V) of solution

Fig. 11. Removal heights of (a) Fe, (b) Co, and (c) Cu workpieces along the radial direction after 3 h of rotary machining